Experimental Study of a High Pressure Rotating Detonation Wave Combustor for Rocket Applications

David Stechmann[1], Dasheng Lim[1], and Stephen D. Heister[2]
Purdue University, West Lafayette, IN, 47906

Abstract
Rotating Detonation Engines (RDEs) represent a promising technology for increasing the specific impulse of rocket combustors, however more research is needed to quantify the real-world performance of these devices and understand how they can be optimized for use at high-pressure conditions. To this end, Purdue University has developed a high-pressure experimental RDE with an oxygen-rich pre-burner capable of operating on liquid methane and liquid oxygen at flow rates up to 9 lbm/sec (4.1 Kg/sec) and mean chamber pressures up to 1200 psi (8.3 MPa). Prior to fabricating the experimental hardware, analysis was undertaken in an effort to understand and quantify overall system flow behavior, injector mixing time lag, injector transient response, and thermal-structural loading. Testing begin in May 2015 with hydrogen, though a transition to higher flow rates with liquid methane is expected in late 2015. Ignition and combustion behavior are reliable and consistent in all tests to date with thrust values reaching approximately 85% of theoretical values. Continuous detonation has not been consistently achieved however and the chamber thermal environment has been especially challenging for instrumentation, so additional design revisions and tests are ongoing.

1. Introduction

During the last half of the 20th century, countless developments in rocket combustor technology led to steady increases in engine performance and efficiency. Since the late 1980s however, innovation has primarily occurred in a few key areas associated with operating economics, reliability, control systems, and manufacturing, while engine specific impulse has changed little. This is no surprise given that combustion efficiencies of modern engines are already near the upper practical limits associated with common propellants. While investments have been made in alternative propellants in an effort to break these limits, most alternative propellants cannot match the handling flexibility or operating economics of existing liquid oxygen and hydrocarbon technology. Given these limitations, significantly new combustor technology is needed to increase performance beyond existing rocket combustors.

Rotating Detonation Engines (RDEs) represent a promising technology for achieving the goal of appreciably increasing rocket engine specific impulse. RDEs are a type of pressure-gain combustion device where most of the combustion takes place in high-pressure detonation waves traveling tangentially around an annular combustion chamber. RDEs can potentially reduce required combustor volume and increase delivered specific impulse by up to 13% (as shown in Figure 1 for methane and oxygen propellants) while avoiding many drawbacks associated with other pressure-gain combustion concepts (including Pulse Detonation Engines). The engineered transient nature of RDEs may also make it possible to avoid unexpected combustion instability during chamber development. This would be a significant boon to engine manufacturers.

---

[1] Graduate Student, School of Aeronautics and Astronautics
[2] Raisbeck Distinguished Professor, School of Aeronautics and Astronautics and Mechanical Engineering

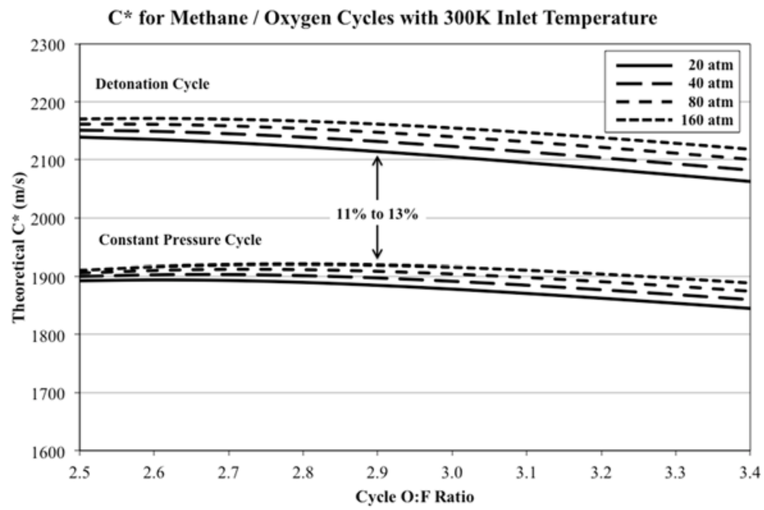

Figure 1: Ideal performance of O_2 / CH_4 for constant pressure and detonation cycle thermodynamic cycles.

2. Design and Operating Parameters

Given the promising nature of Rotating Detonation Engine technology, Purdue University initiated a RDE research effort in August 2014 sponsored by the U.S. Air Force Office of Scientific Research. The primary objective of this research was to assess the operational challenges and performance advantages of a RDE combustor for rocket vehicle applications. To this end, a high-pressure rotating detonation engine article has been developed and installed at Purdue University's Zucrow Laboratories and is capable of operating at flow rates close to 9 lbm/sec (4.1 Kg/sec) and at mean chamber pressures close to 1200 psi (8.3 MPa) using liquid methane and liquid oxygen propellants. Additional details regarding the operating parameters associated with this RDE are shown in Table 1 and Figure 2.

Table 1: General design and operating parameters for the RDE test article

	42% Throttle	67% Throttle	100% Throttle
Total Mass Flow (lbm/sec)	3.73	5.95	8.89
Design Mean Channel Pressure (psia)	504	804	1200
Methane Manifold Pressure (psia)	575	1025	1725
Methane Mean Injection Velocity (ft/s)	156	250	368
Detonation Pressure Ratio	34.14	34.48	34.76
Max Shock Pressure (psia)	6195	9979	15017
Detonation Velocity (ft/s)	8790	8838	8880
Min Expected Operating Frequency with 1 wave (kHz)	8.68	8.73	8.77
Max Expected Injector Cycle Time with 1 wave (μs)	115.2	114.6	114.1
Expected C* - CP mode (ft/s)	6227	6248	6266
Expected C* - Det mode (ft/s)	6945	6976	7003
Expected Thrust without divergent nozzle - CP mode (lbf)	872	1408	2119
Expected Thrust without divergent nozzle - Det mode (lbf)	972	1572	2368

While a great deal of detonation engine research has focused on air-breathing systems with other fuels, liquid oxygen and liquid methane were selected in this application for their potential relevance to launch vehicle propulsion systems. Maximum flow rates were driven by limitations associated with the high-pressure liquid methane facilities already available at Zucrow Laboratories, and maximum mean chamber pressure was set by the desire to obtain conditions similar to existing rocket combustors while still being capable of operating for reasonable periods of time using heat-sink cooling. The maximum mean chamber pressure value was also driven by the desire to explore operational regimens and pressures above those typically characterized in prior research.

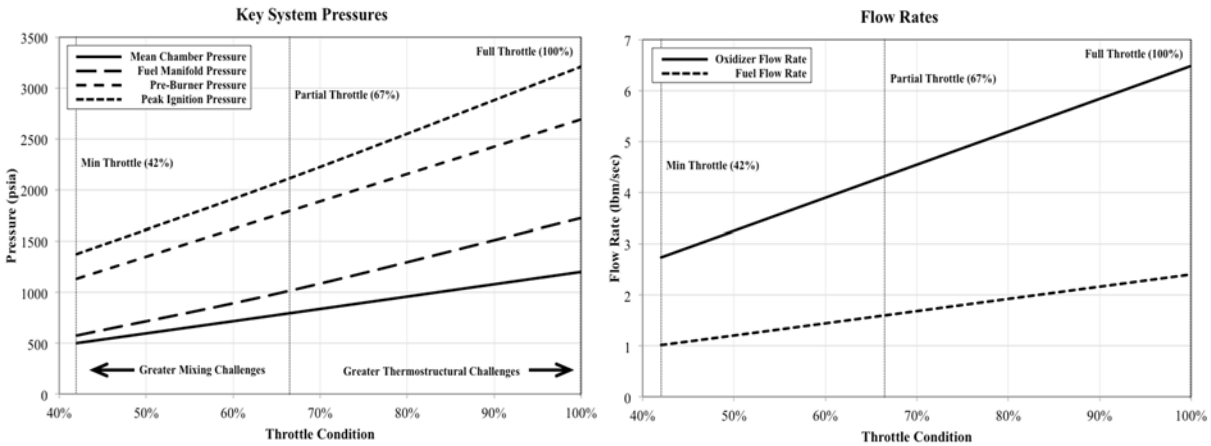

Figure 2: Design pressures (left) and flow rates (right) associated with the experimental RDE.

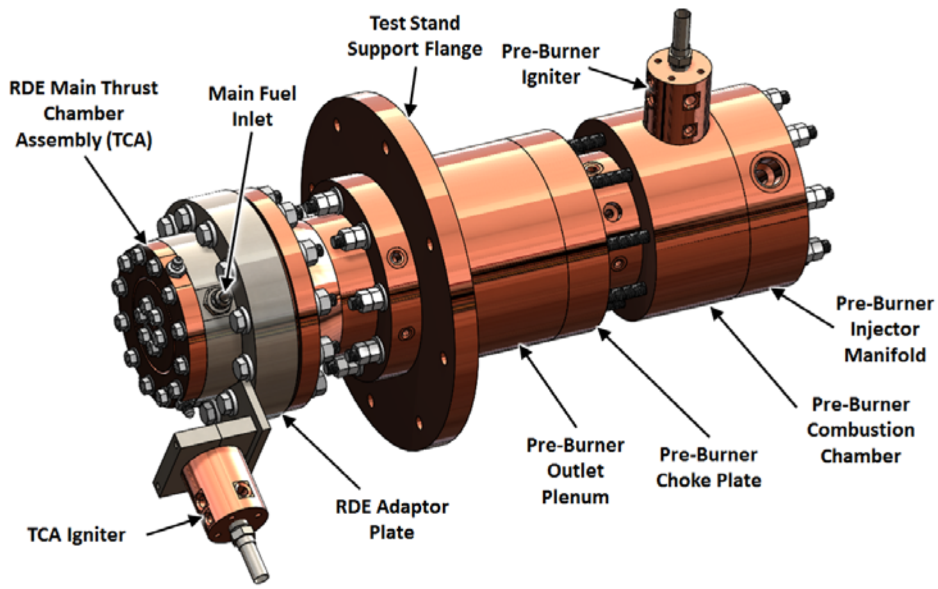

Figure 3: An overview of the test article showing primary elements of the oxygen-rich pre-burner and the main rotating detonation engine subassemblies. The test article is approximately 26" (66 cm) long.

An overview of the test article layout used for this research is shown in Figure 3. The test article can be divided into two primary subassemblies: a constant-pressure oxygen rich pre-burner and a main RDE attachment. The pre-burner consists of an injector, a combustion chamber, a choke-plate (to minimize coupling between the RDE and pre-burner combustion chamber behavior), an exit plenum, and a test stand support flange. The pre-burner is manufactured primarily using copper with appropriate thermal barrier coatings to facility relatively long-duration operation without the need for active cooling. While the pre-burner adds complexity to an otherwise smaller RDE test assembly, this approach more closely represents a closed-cycle rocket engine design application and facilitates mixing of the propellants. Due to the very rapid cycle time in a detonation engine of this size (around 120 microseconds for one wave), mixing time-scales will be very small and any delay associated with propellant vaporization could be problematic. The selected approach makes it possible to burn the liquid oxygen in a high O:F environment in the pre-burner and produce hot oxygen rich gas than will mix with and vaporize the liquid methane within the time-scales needed for operation.

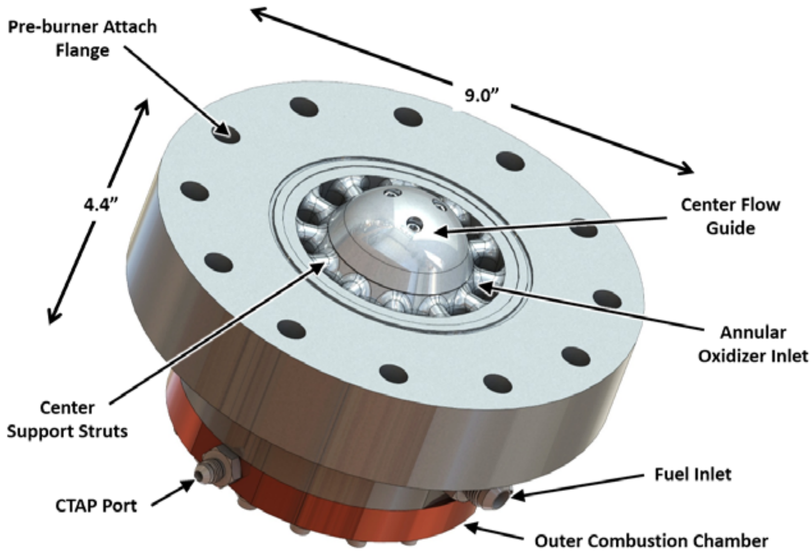

Figure 4: A perspective view of the RDE subassembly from the oxygen inlet side connected to the pre-burner.

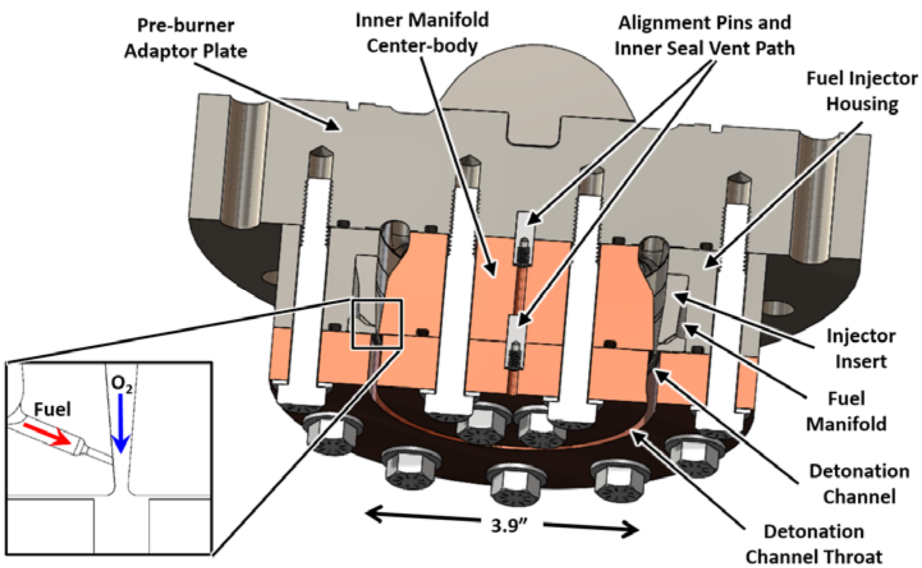

Figure 5: A section view of the RDE subassembly. The fuel and oxidizer flow path are highlighted on the left.

The RDE subassembly is shown in detail in Figure 4 and in cross section in Figure 5. This subassembly is approximately 9" (23 cm) in diameter and approximately 4.4" (11.2 cm) long and consists of an adaptor plate with a center support structure and flow guide that is bolted to the pre-burner, a fuel injector, an outer copper combustion chamber, and two inner copper center-body components that form the inner wall of the detonation channel and annular flow-path. All thrust loads from the RDE are transferred through the adaptor plate and into the pre-burner. The outer diameter of the detonation channel is 3.87" (9.83 cm), the channel width is 0.15" (3.8 mm) and the channel length from injector face to nozzle exit is 0.75" (1.9 cm). The outer diameter was sized so it would be compatible with the pre-burner outlet plenum (to avoid turning of the flow). The outer diameter was also selected to provide optimal expansion of the flow at the desired maximum pressure if an aerospike nozzle was attached and to provide enough central space for bolts and seals. The channel width and length were selected to match the desired flow rates, the expected chamber L* values (which can be smaller in a detonation cycle by an order of magnitude), and the expected instrumentation and igniter port geometry. [1] The width and length were also selected to be compatible with the cell size and fill height criteria established in prior research. [2] Once again, copper was used for the chamber and center-body parts to facilitate operation for short periods of time (1 to 3 seconds) without active cooling. No thermal barrier coating was used on the copper chamber because it was not considered necessary for the short duration tests planned and because the durability of the coating in the chamber environment was questionable.

Both the pre-burner and the main detonation channel employ torch ignition systems driven by gaseous oxygen and hydrogen. While many detonation engines have been started using explosives or small pulse-detonation engines attached to the main detonation channel, recent studies have also indicated that simple torch-style ignition of an annular combustor can work if enough time is allowed for naturally occurring tangential instabilities to grow. [3] A torch ignition system was consequently selected for the Purdue RDE to provide more benign start transients.

Within the RDE subassembly, precision alignment pins are employed on the outer and inner components to ensure consistent flow-path area around the annulus once all components are assemble. The inner alignment pins are ported to provide a vent flow-path for the back-side of the internal seals. A straight convergent flow-path from the pre-burner, through the center support struts, and through the fuel injector is employed for the oxidizer to minimize pressure losses and flow turbulence associated with turning the high volumetric flow rate from the pre-burner. As shown in Figure 5, this path converges through a narrow annular choke just prior to entering the main detonation channel. Fuel is injected just upstream of this choke to provide fast mixing and vaporization of the fuel and oxidizer in the high velocity gas flow. It should be noted that the oxidizer flow-path geometry employed in this test article is appreciably different from the serpentine flow-path used on some well-studied prior air-breathing test articles. [4]

The fuel injector itself consists of an outer annulus and an inner insert that are jointed together using Electron-Beam (EB) welding after the parts are machined to provide a high-strength leak-free joint. Brazing was originally tried on this assembly, but challenges with the material necessitated a switch to EB welding. The fuel manifold is located between the two parts and is sized to keep dynamic head less than 1% of static head during operation. This keeps the flow velocity low enough to minimize unequal distribution within the manifold. The manifold is small enough however to keep velocity high enough to facility back-face cooling. Back-face cooling is important to minimize the potential for fuel vapor lock when running at lower pressure conditions with subcritical liquid methane.

At the lower end of the manifold on the fuel injector insert, 120 fuel orifices 0.020" (0.5 mm) in diameter are drilled at 3-degree intervals using small-hole EDM. The orifices are sized to provide the desired full-engine O:F of 2.7 at the maximum flow condition and mean chamber pressure of 1200 psi (8.27 MPa) while remaining within the pressure limits associated with the liquid methane feed system upstream of the venturi. The slight orifice drill angle is set to allow access to the part from the EDM machine. The fuel orifice lengths and the convergent geometry are sized to provide the desired dynamic response to a detonation wave while keeping viscous losses to a minimum. If the fuel orifices were too long, then the viscous losses would be excessive and the fuel flow would not fluctuate or briefly stop as needed during detonation wave passage. If the fuel orifices were too short, then the detonation-wave could force chamber exhaust gasses into the fuel manifold – an undesirable condition. As documented later, a dynamic analysis was used to size this distance to 0.08" to ensure the desired dynamic response.

Several sealing grooves are included in the design as shown in Figure 5, and these grooves are designed to house 1/8" spring-energized copper-coated Inconel C-rings. This sealing approach was chosen for its compatibility with the oxygen-rich gasses present in the RDE subassembly and pre-burner, the potential large temperature swings from cryogenic to combustion chamber gasses, the minimal desired seal leak rate, the groove manufacturing tolerances, and the hardness of the mating surfaces. The pre-load required for this type of seal is also consistent with recommendations for rocket applications in prior literature. [5] While this type of seal can handle the extreme environmental conditions well, the seal locations are still placed as far as possible from the detonation channel to minimize temperature excursions and maximize longevity. The grooves themselves are also placed facing a consistently upward orientation based on the anticipated assembly procedure so this procedure would be easier to follow in practice. It should be noted that pains were taken during the design process to limit the number of unique C-ring sizes to only two so the cost and lead-time associated with these very specialized seals could be minimized. It should also be noted that in addition to the spring-energized C-rings, the grooves were also designed to be compatible with standard 1/8" Viton O-rings for low-pressure tests without cryogenic fuel.

Both the adaptor plate and the fuel injector are built from 17-4PH – a martensitic high-strength stainless steel. Prior to machining high-tolerance features like the alignment pin holes and O-ring grooves, both components are age-hardened to an over-aged condition. While this reduces strength somewhat from the maximum attainable value, the strength is still quite appreciable and this process increases fracture toughness – a desirable characteristic for parts that will be exposed to cryogenic conditions and large thermal transients.

The main RDE detonation channel employs a geometric throat at the nozzle exit and a contraction ratio of 1.25. A geometric throat was included to provide consistent choking around the annulus and to increase the mean chamber pressure. The throat area is sized by the expected mean chamber pressure, mass flow rate, and characteristic velocity of the exhaust gasses (C*). This sizing is identical to what would be done for a constant-pressure combustion chamber. The contraction ratio is kept relatively small to maximize the thrust that can be extracted from the transient nature of the detonation wave (since it is thought that a high contraction ratio would reduce the benefits to simply that of a constant pressure cycle). It should be noted that there is still some uncertainty as to whether a convergent divergent nozzle or simply a divergent nozzle is best for an RDE, so several different chamber geometries will be tested in the course of this research by machining different chamber center-body components. [6]

An additional important area of the RDE design relates to instrumentation and data acquisition. While thorough data acquisition is important for characterizing RDE performance and operating behavior, a minimum instrumentation suite was employed in the test hardware until initial testing could be completed. This minimal instrumentation suite consists of a CTAP (capillary tube averaged pressure) for measuring the mean detonation channel pressure, a flush-mounted PCB transducer for measuring high-frequency pressure response in the detonation channel, an flush-mounted ion-gage for measuring high-frequency flame front propagation in the detonation channel, load cells for measuring axial thrust, a calibrated microphone for evaluating the engine and exhaust acoustic signature, a high-speed camera and mirror assembly for viewing combustion through the nozzle, and low-speed cameras for taping and photographing the test and exhaust plume.

3. Analysis and Operating Parameters

For the most part, the design and analysis approaches used in developing and evaluating this RDE have been similar to techniques and methods employed in any rocket engine. In particular, much of the flow-system has been designed using mean-pressure and mean-flow rate assumptions. These assumptions should be fairly accurate in most areas of the design not subjected to the detonation wave, and as such they will not be described in detail here. In areas of the design where either transient detonation behavior or the annular geometry will have a significant affect on operating characteristics, NASA CEA or more specific techniques related to detonation cell size, injector mixing, injector dynamic response, and chamber thermal and structural analysis were employed.

3.1 Detonation Cell Size Analysis

RDE operating behavior can be highly dependent on the relationship between the detonation cell size and some of the key geometric parameters including fill height per cycle, detonation channel width, channel length, and channel diameter. [2] In order to gauge the effects these parameters would have on this engine, GALCIT data for both hydrogen / oxygen and methane / oxygen was collected and extrapolated into the pressures where this engine is expected to operate. The data distribution and the results of the extrapolation are shown in Figure 6. It is clear from the distribution and the extrapolations that this engine will generally operate in a regimen where the detonation cell size is exceedingly small. The results of the extrapolation are reflected in Table 1 above. Based on the extrapolated cell sizes and criteria established in prior literature, it is clear that no geometric aspects of this engine should be limited by the cell size. [2] It is also clear from reviewing prior literature that the optimal chamber lengths (based only on the cell size) may be very short – too short to easily install instrumentation and the torch ignition system. As such, the chamber length was sized more by other considerations (as noted earlier) than by any cell size limits.

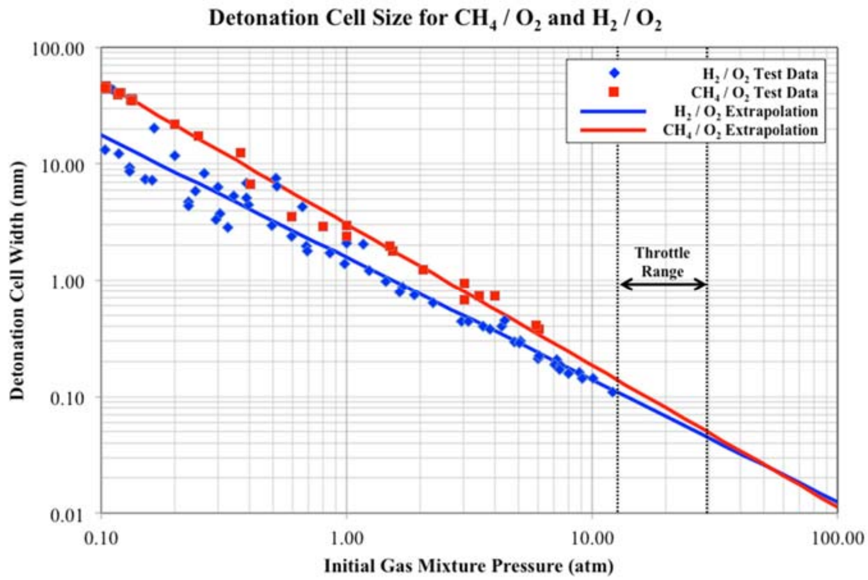

Figure 6: GALCIT detonation cell size data for hydrogen / oxygen and methane / oxygen. The extrapolations and the operating range of the RDE test article are shown.

3.2 Mixing Analysis

Due to the very fast detonation cycle times in a RDE this size (~120 microseconds for a single wave as noted in Table 1), mixing was a very significant challenge. This was one of the factors that drove the decision to use a pre-burner, but even with this it will still be challenging to break-up the liquid methane jet, vaporize the resulting droplets, and mix the resulting gas with the pre-burner gas in a timely fashion. To evaluate the total time required by this process and set the maximum methane orifice size for efficient mixing, each step in the injection process was considered in turn. In the first step, the methane behavior was evaluated as a simple jet-in-crossflow, and the correlation employed by Tambe was used to estimate the overall trajectory. [7] The results of this model are shown in Figure 7 (left). The results of this analysis suggest that even with small orifices, much of the liquid methane jet will cross through the annular pre-burner flow and impact on the opposite wall a very short distance away.

As the methane jet impacts the wall immediately opposite of the fuel orifice, it will splash with a characteristic fluid sheet thickness that can be computed according to Ashgriz. [8] The sheet thickness at these impact velocities and impingement angles based on this model is shown in Figure 7 (right). This distribution suggest that while the distribution in sheet thickness will likely be the most uniform at the highest impact velocity and highest throttle setting, the sheet thickness in all cases is not especially high. In general the droplet size that will emerge from a sheet should be on the same size scale as the sheet thickness, and since this droplet will still be exposed to the high-velocity pre-burner flow, it is possible to estimate the droplet breakup time and secondary droplet diameter. [9] The results of this analysis are shown in Figure 8.

At this point it is possible to compute the secondary droplet vaporization delay using convective heat transfer coefficients for an ideal sphere in cross-flow and a lumped-parameter methane vaporization model based on energy input. The details of this model are beyond the scope of this document, but the results of this computation for the three throttle cases are shown in Table 2 along with the estimated time for each prior step. While this analysis is admittedly rather simplistic and idealistic in nature given the complexity of the flow behavior, the intention is only to give a very approximate assessment of mixing times in an injector like this. The results seem to suggest that at low throttle settings the mixing delay may take up a significant fraction of the total cycle time while at high throttle settings it should represent a much smaller fraction of the total cycle time.

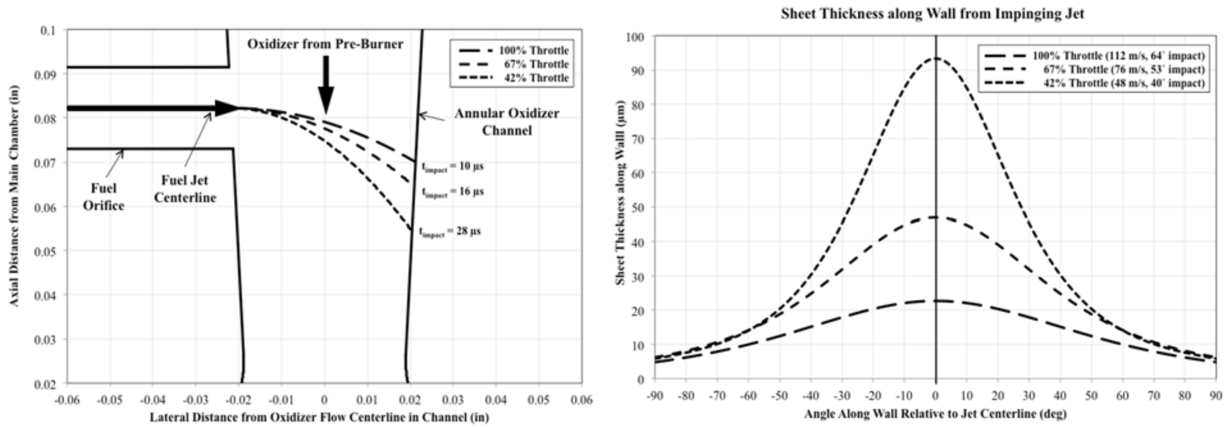

Figure 7: Methane jet injection behavior (left). Methane splash sheet thickness on the opposite wall (right).

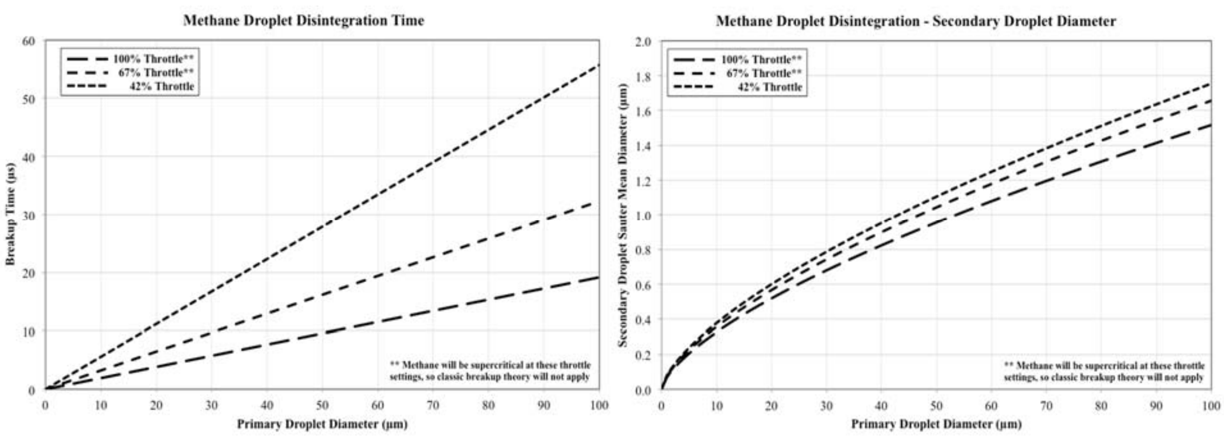

Figure 8: Methane droplet disintegration time (left) and secondary droplet diameter (right).

Table 2: Estimated methane jet mixing time

	42% Throttle	67% Throttle	100% Throttle
Fuel Jet Travel (µs)	28	16	10
Splash Spreading / Rebound (µs)	15	10	7
Droplet Breakup (µs)	25	8	3
Droplet Vaporization (µs)	2	1	<1
Total Estimated Mixing Time (µs)	70	35	21

3.3 Injector Dynamic Response Analysis

The results of the approximate mixing analysis shown in section 3.2 suggest that it will be possible to inject and vaporize methane within the time scales of a single detonation cycle, however this analysis ignores one very important characteristic: the injectors themselves will respond to the detonation wave and will take some time to recover. Additionally, the different densities and supply pressures of the methane and the oxygen make it likely that the injectors will not respond in the same way and will either cease flowing or begin flowing again at different points in time. This may lead to an unfavorable spatial-variation in O:F in the combustion chamber that will adversely affect performance or operability.

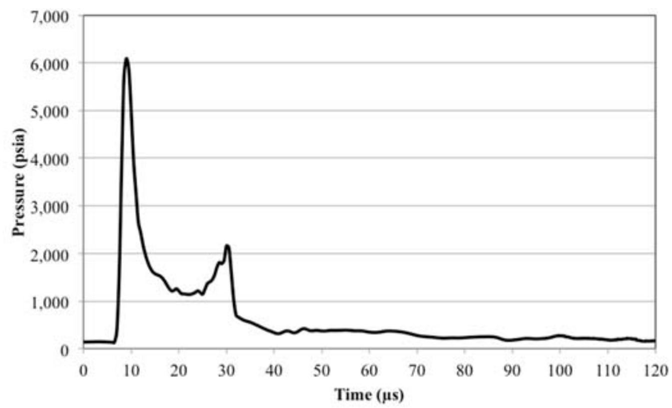

Figure 9: Detonation pressure profile at the injector face of a gaseous oxygen / gaseous methane RDE based on a 2D unwrapped CFD model using finite-rate chemical kinetics.

To evaluate this behavior in more detail and adjust supply pressures or geometry to compensate, several numerical models were created for the different orifices and boundary conditions in question. The first model represented the RDE channel as a 2-dimensional unwrapped domain and employed compressible CFD with finite-rate chemistry to generate a non-idealized detonation pressure profile. This pressure profile is shown in Figure 9. The secondary pressure spike is due to delayed reaction from some of the propellant. While the details of the analysis model are outside the scope of this paper, it should be noted that the purpose of this analysis was to generate an approximate profile that could be used as a transient boundary condition for more detailed injector orifice response models.

The second model represented the oxidizer orifice as an ideal 1-dimensional channel and employed compressible CFD along with the applied transient pressure profile shown in Figure 9 to evaluate oxidizer back-flow distance, transient mass flux, and orifice response time. This model was also used with hydrogen to evaluate the effects of flowing hydrogen through the fuel manifold instead of liquid methane during initial testing with the original hardware and with modified hardware. Finally, the third model represented the fuel orifice as an ideal 1-dimensional channel and employed a lumped-parameter approach along with the aforementioned transient pressure boundary condition to evaluate back-flow in the liquid methane. The combined transient orifice back-flow behavior computed by these models is shown in Figure 10 for the fuel orifice with methane, the fuel orifice with hydrogen, a modified version of the fuel orifice with hydrogen, and the oxidizer channel.

In Figure 10, the original fuel orifice with methane and the modified fuel orifice with hydrogen are referred to as "matched" because they represent final versions of the design that were already adjusted to better match the response of the oxidizer orifice. This can be seen by looking at the response of the original (unmodified) orifice with hydrogen. In this case the hydrogen returns significantly before the oxidizer. The matched hydrogen orifice responds at nearly the same time as the oxidizer. The matched methane orifice appears to lag significantly, but this is actually the best option tested with the computational model. The primary parameter that affected response behavior in the methane orifice was the orifice depth. Deeper orifices didn't appear to experience the same amount of back-flow and in some cases didn't cease flowing at all (likely due to the large momentum behind the column of fluid in the orifice) while shorter orifices experienced more significant backflow and in many cases lagged the oxidizer even more. Neither option was desirable, so based on these rough calculations we decided upon a methane orifice length of 0.08" – the value associated with the matched response line in Figure 10.

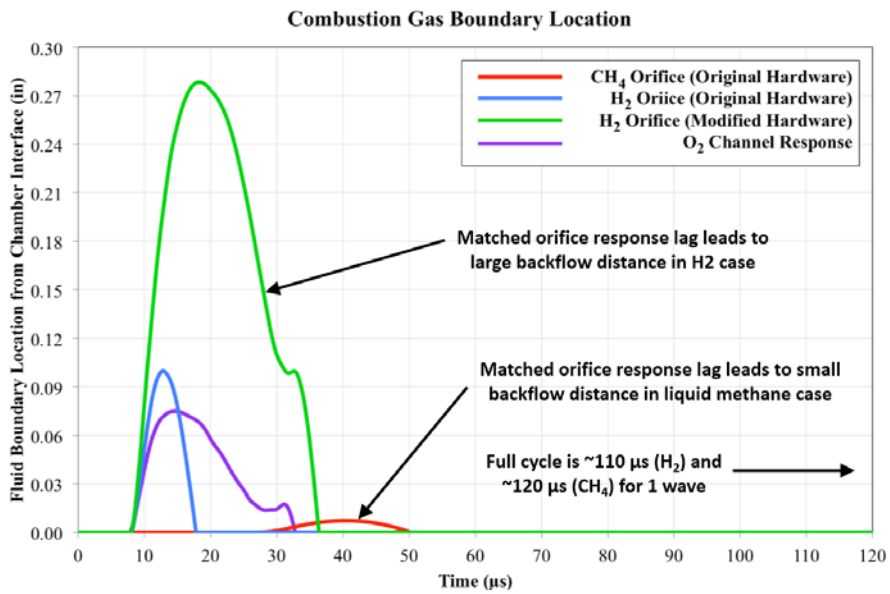

Figure 10: Transient orifice response behavior based on numerical results. The "matched" fuel orifices refer to orifices where geometric changes were made so the fuel response would better match the oxidizer response.

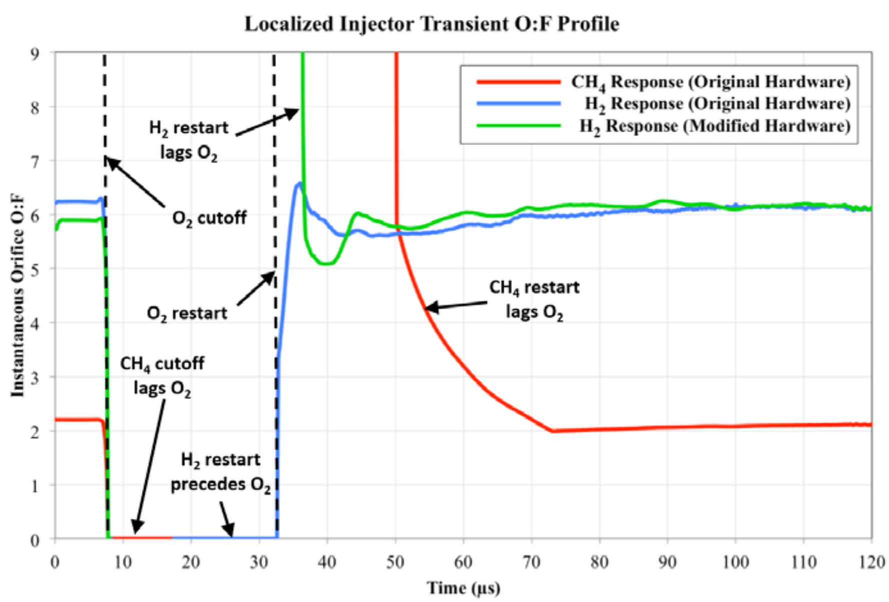

Figure 11: Transient O:F profile in the RDE for different orifices and fluids due to back-flow behavior.

Based on the 1D lumped parameter and CFD orifice response models, it was possible to compute transient mass flux in addition to the back-flow behavior. From this it was possible to adjust orifice sizing slightly to ensure the total cycle O:F remained at approximately 2.7 for methane and approximately 6 for the trial case with hydrogen. Using the refined orifice dimensions and transient mass flux data, it was also possible to derive the transient O:F profiles to evaluate mixing temporally. The results of this analysis are shown in Figure 11. It should be noted that the hydrogen curves tend to be more variable due the shock behavior in the compressible CFD model where the methane lumped parameter model does not capture this effect. It should also be noted that while these models are rather simple given the complex geometry, the objective was solely to give an approximation of the back-flow behavior and temporal mixing profile in the RDE. When these results are combined with the results from section 3.2 for jet breakup and vaporization, it is clear that while the complete mixing process should be able take place on the time-scales needed, the two effects combined will likely take up much of the 120 micro-second cycle in this RDE.

3.4 Structural and Thermal Analysis

Due to the high pressures and high thermal loads associated with a RDE at the desired conditions noted earlier, thermal-structural analysis and structural optimization was a critical part of the design process. In general, a simple yet conservative approach was employed for this process and only three load case were considered for all RDE components: Peak ignition over-pressure (which assumes the entire channel detonates at once which would produce approximately 3200 psi), nominal chamber pressure (1200 psi) with 100% throttle heat flux calculated at the point where the inner copper wall beings to melt (approximately 0.8 seconds), and minimum chamber pressure (500 psi) with minimum throttle heat flux calculated at the point where the inner copper wall beings to melt (approximately 2.5 seconds).

In general the copper RDE chamber components were sized by the high heat flux short-duration thermal case. While heat-flux in RDEs is not well understood, a conservative value was created for this analysis based on the mean chamber pressure, combustion gas temperature, and an assumed constant chamber Mach number of 1.0 (which would be overly conservative for most of the chamber most of the time).

In general the adaptor plate and injector were sized by the peak over-pressure case. The adaptor plate and the injector were the most challenging components structurally and ultimately necessitated the use of 17-4PH high-strength stainless steel. Worst-case stresses on the injector were due to the large pressures and large thermal gradients between the cryogenic liquid methane and the hot pre-burner gas. The safety factor distribution associated with the injector housing is shown in Figure 12 (left). The worst-case adaptor plate stresses were due to several factors including the nature of the central support strut geometry (which limited the amount of material that could join the inner and outer body due to the internal flow-path), the O-ring placement relatively far from the combustion chamber annulus, the potential for high peak over-pressures at ignition, the C-ring pre-load, and the uncertainty associated with bolt clamp-up. In addition, the adaptor plate structure was overdesigned relative to the central center-body bolts so a catastrophic over-pressure would cause these bolts to fail first. In this way, the hardware was designed to act in a fail-safe manner in case of overload by blowing off the chamber center-body and relieving pressure to protect the pre-burner, the fuel injector, the adaptor plate, and the instrumentation embedded in the chamber wall. The safety factor distribution associated with the worst fail-safe case on the adaptor plate is shown in Figure 12 (right). Note that all of these analyses use ultimate load values (1.5 times worst-case design loads), and all analysis use non-linear material properties that account for material property changes at temperature.

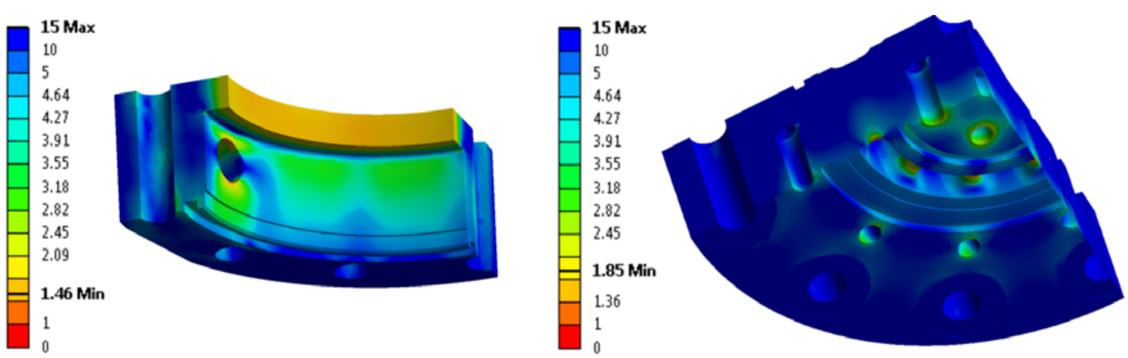

Figure 12: Injector housing safety factor (left) and adaptor plate safety factor (right).

4. Test Facility Overview

The facility that has been configured to support RDE testing at Purdue's Zucrow Laboratories consists of three primary subsystems: the methane liquefaction and supply system, the liquid oxygen supply system, and the gaseous hydrogen / gaseous oxygen supply system for the igniters. During test preparation, gaseous methane is forced through a methane liquefaction loop into a run tank jacketed with liquid nitrogen. The liquid nitrogen makes it possible to liquefy the methane and control the overall methane temperature. At the same time, gaseous methane is pumped from low-pressure storage bottles to 6000 psi (41.3 MPa) and stored. During engine firing, liquid methane is forced from the jacketed run tank by high-pressure gaseous methane into the RDE main fuel manifold. A schematic of this system is shown in Figure 13 (left).

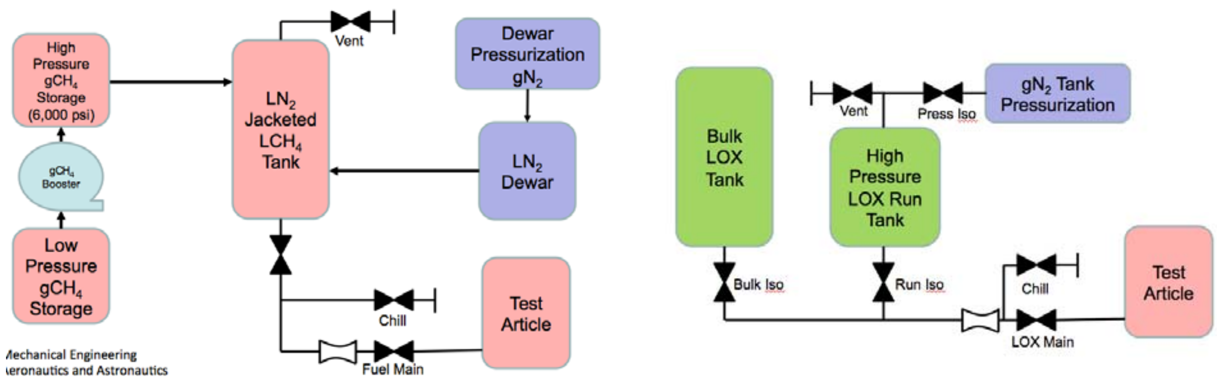

Figure 13: The Zucrow high-pressure liquid methane system (left) and liquid oxygen system (right).

The liquid oxygen supply system shown in Figure 13 (right) consists of a low-pressure bulk liquid oxygen storage tank, a high-pressure liquid oxygen run tank, and a high-flow gaseous nitrogen pressurization system. During test preparation, liquid oxygen is forced from the low-pressure bulk storage tank into the run tank at low-pressure. Liquid oxygen from the run tank is subsequently forced at low-pressure through lines to the test article to chill the feed system. During testing, gaseous nitrogen is used to pressurize the run tank and force liquid oxygen into the pre-burner. Overall the system is capable of supplying liquid oxygen at up to 5000 psi and up to 15 lbm/sec if necessary.

The gaseous hydrogen and gaseous oxygen supply system consists of high-pressure oxygen bottles, a 5000 psi 20 cubic foot bulk hydrogen storage tank, and a 6000 psi high-pressure nitrogen purge system. A schematic of this system is shown in Figure 14. During testing, gaseous oxygen and gaseous hydrogen are forced into the igniters for the pre-burner and the main detonation channel in sequence with a spark to ignite the respective chamber. Hydrogen is also used directly from this system as the main fuel source for the oxygen-rich pre-burner.

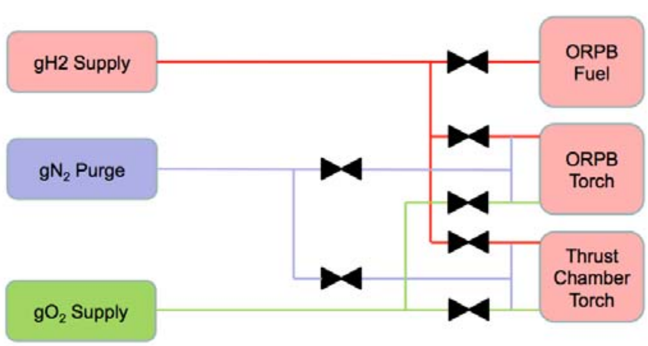

Figure 14: The Zucrow gaseous oxygen and gaseous hydrogen feed system for the igniters and pre-burner.

5. Test Results

As of this writing, 35 RDE and pre-burner tests have been completed (most of these being hot-fire tests). While the test article was designed for use with liquid methane, all of these tests were conducted using gaseous hydrogen instead to establish a baseline before moving to a more difficult fuel. Starting with hydrogen also made it possible to test sooner due to the easier facility integration. Due to the very different densities between hydrogen and liquid methane, a new center-body was built for these tests. This new center-body was designed to reduce the channel and throat width to 0.12” (3.05 mm) and 0.053” (1.35 mm) respectively. Viton O-rings were also used instead of the more expensive metal C-rings since the RDE subassembly did not need to withstand cryogenic temperatures during testing with hydrogen. The injector assembly used with the first set of tests was originally brazed before being welded (due to quality issues with the material supplier), and as such it had to be used in non-heat-treated condition.

It is clear from the first set of hot-fire tests that the pre-burner and torch ignition system function as intended. In general the test sequence begins by purging the hardware with nitrogen, flowing liquid oxygen through the pre-burner to chill the manifold, purging with nitrogen again, and then starting the pre-burner torch igniter. Once the igniter has reached optimum pressure (100 to 200 milliseconds), the main pre-burner propellant valves are opened. After the pre-burner has lit and reached a consistent outlet temperature near 430 F (approximately 500K), the main torch igniter connected to the detonation channel is lit. After this igniter has reached optimum pressure, the main hydrogen valve to the RDE fuel manifold is opened. This valve closes shortly thereafter leading to approximately 1 second of total burn time in the main detonation channel. A firing time of one second was selected to balance the need for data acquisition at steady-state operation with the desire to minimize thermal loads on the hardware.

To date, all tests have focused on total flow rates of approximately 0.45 lbm/sec (0.2 Kg/sec) and 0.9 lbm/sec (0.4 Kg/sec) at equivalence ratios between 0.4 and 1.6. Additional test series are planned at 1.35 lbm/sec and 1.8 lbm/sec with hydrogen before transitioning to methane as shown in Table 3. In general, the RDE ignites consistently and reliably at all conditions, and it is clear from high-speed camera footage that this ignition propagates at near CJ velocity around the annulus. The mean chamber pressure increases during these tests as expected and tends to consistently reach the target pressure value approximately 200 milliseconds after ignition. At this point the mean chamber pressure continues to climb slowly until shutdown. This behavior can be seen in Figure 15 for a typical test. The gradual increase in mean chamber during much of the remaining burn is likely due the increasing copper wall temperature. This increasing wall temperature reduces the energy deposited into the wall thereby reducing the cooling effect of the wall on the gas. It also leads to thermal expansion, and since the inner center-body heats up faster than the outer annulus due to the geometric profile, the total throat area contracts slightly during the burn.

Table 3: The planned RDE test series with hydrogen before transitioning to liquid methane

Test Series	OD (in)	Gap (in)	L/Gap	φ	mdot (lbm/sec)	Pc (psia)	Deliv. C* (ft/s)	Theor. C* (ft/s)	C*_del/ C*_th (from thrust)	L* (in)
1	3.87	0.12	6.3	0.4 – 1.6	0.45	150	4460*	6977	~64%**	1.7
2	3.87	0.12	6.3	0.4 – 1.6	0.9	300	5900	7036	~84%	1.7
3	3.87	0.12	6.3	0.4 – 1.6	1.35	450*	TBD	7072	TBD	1.7
4	3.87	0.12	6.3	0.4 - 1.6	1.8	600*	TBD	7095	TBD	1.7

* Expected pressure value – test has not been completed yet.
** Thrust measurement is less accurate the low flow test case.

While mean chamber pressure tends to climb gradually during testing, thrust quickly climbs at ignition and settles at a mean value that tends to be approximately 80% to 85% of the theoretical maximum thrust predicted. This can be seen for the same test condition in Figure 16. Tests at the lower flow rate of 0.45 lbm/sec tend to produce smaller thrust value relative to the predicted maximum theoretical value, but the low flow rate and the large plumbing stiffness mean that these thrust values tend to be under-predicted somewhat.

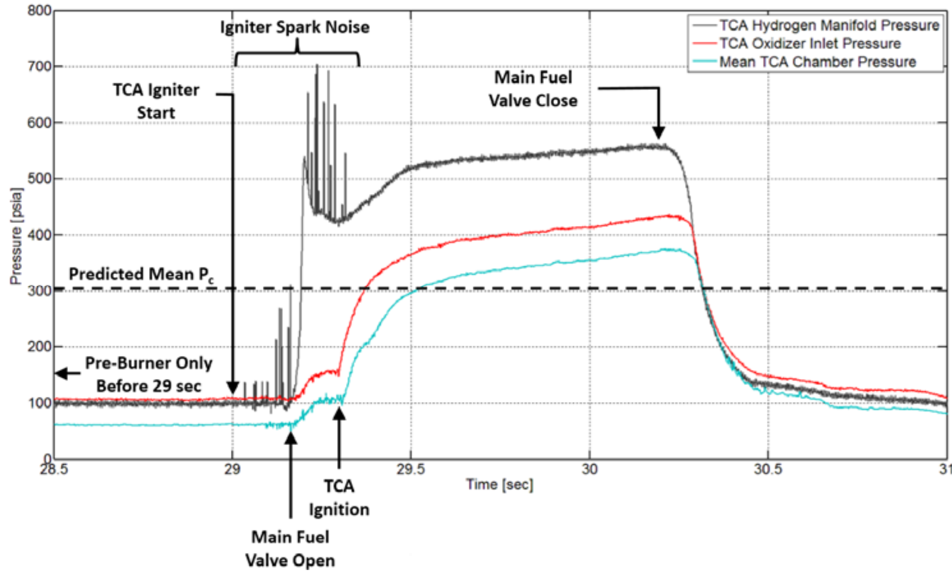

Figure 15: RDE pressure behavior during a test at 0.9 lbm/sec and φ = 1.0. The general behavior observed during this test is typical of all RDE tests to date.

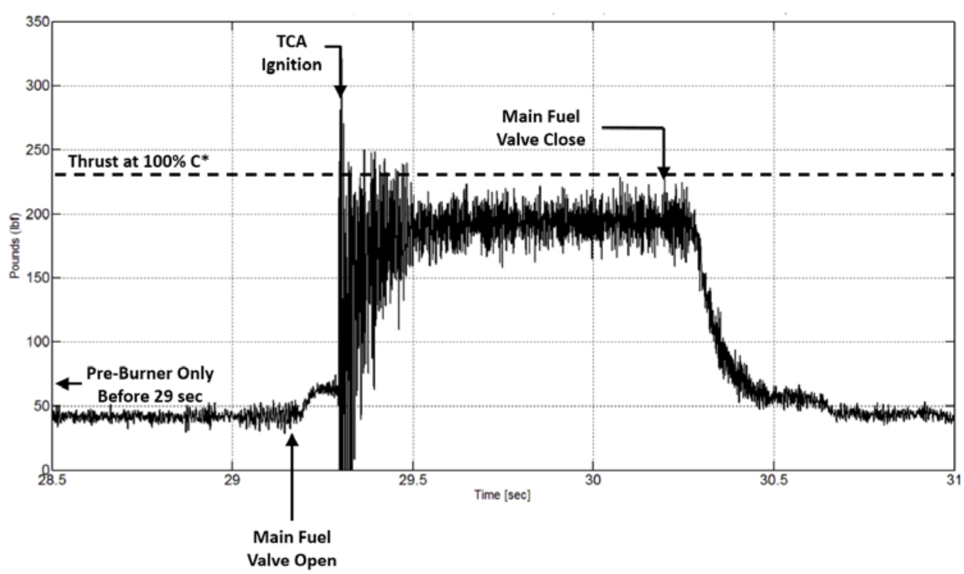

Figure 16: RDE thrust during a test at 0.9 lbm/sec and φ = 1.0. The general behavior observed during this test is typical of all RDE tests to date.

While the mean chamber pressure and thrust observed during testing appear to be follow predictions fairly well, the high-speed footage, microphone data, and load cell data do not appear to show the expected resonant frequencies associated with detonation until right at shut-down. This can be seen in the spectrogram shown in Figure 17 for the same test as the data shown above. As before, this plot is typical of all tests to date. Data from the flush-mounted PCB microphone and ion probe are also suspect due to thermal overloading in the high heat-flux environment. While these results are still preliminary and more testing is scheduled in the near future, it appears likely that the primary behavior at this point is simply turbulent combustion. If detonations are occurring, it is likely they are only occurring near shutdown. Work is still ongoing on understanding this behavior.

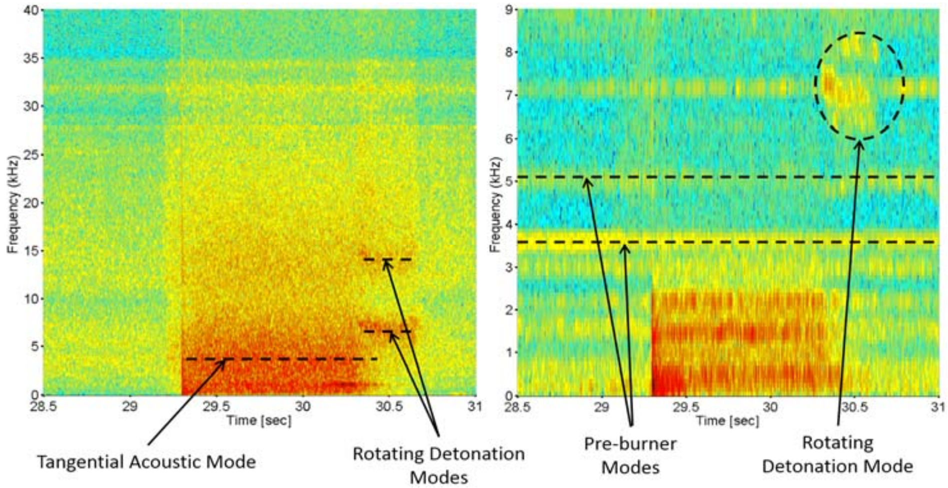

Figure 17: Microphone spectrogram (left) and load cell spectrogram (right) data from a test at 0.9 lbm/sec and φ = 1.0. The general behavior observed during this test is typical of all RDE tests to date except test 35.

6. Conclusions and Future Work

Purdue has designed and constructed an experimental RDE and pre-burner assembly at the Maurice Zucrow Laboratory complex for conducting high-pressure rotating detonation engine tests using liquid methane and liquid oxygen. Analysis prior to testing focused on overall mean fluid system performance and sizing, propellant mixing, transient injector response, and hardware thermal / structural analysis. Initial testing has focused on moderate pressure and low flow operation using gaseous hydrogen and liquid oxygen before transitioning to liquid methane. While ignition and combustion appear consistent in all tests to date, detonation behavior has not been consistently observed in the test article and only appears near shutdown. Testing is ongoing in an effort to better understand this.

Acknowledgements

The authors would like to thank Brandon Kan, Michael Bedard, Scott Meyer, Robert McGuire, and Jarad Neal for their invaluable advice, technical support, facility operation, and manufacturing expertise. The authors would also like to thank the U.S. Air Force and NASA's Marshall Space Flight Center for their support.

References

[1] Stechmann, D., Lim, D., Heister, S. D., Survey or Rotating Detonation Wave Combustor Technology and Potential Rocket Vehicle Applications, *AIAA 50th Annual Joint Propulsion Conference and Exhibit*, 2014.

[2] Bykovskii, F. A., Zhdan, S. A., and Vedernikov, E. F., Continuous Spin Detonations, *Journal of Propulsion and Power,* Vol. 22, No. 6, 2006, pp. 1204–1216.

[3] Bykovskii, F. A., Zhdan, S. A., and Vedernikov, E. F., Initiation of Detonation of Fuel–Air Mixtures in a Flow-Type Annular Combustor, *Journal of Combustion, Explosion, and Shock Waves*, Vol. 50, No. 2, pp. 214-222.

[4] Naples, A., Hoke, J., Schauer, F., Rotating Detonation Engine Interaction with an Annular Ejector, AIAA *52nd Annual Aerospace Sciences Meeting*, 2014

[5] 3. Huzel and Huang, "Design of Liquid Propellant Rocket Engines," AIAA, 1992.

[6] Lu, F., Braun, E., Massa, L., and Wilson, D., "Rotating Detonation Wave Propulsion: Experimental Challenges, Modeling, and Engine Concepts", *Journal of Propulsion and Power*, Vol. 30, No. 5, 2011.

[7] Tambe, S. B., Jeng, S. M., Mongia, H., Hsiao, G., Liquid Jets in Subsonic Crossflow, *AIAA 43rd Annual Aerospace Sciences Meeting*, 2005.

[8] Sarchami, A., Ashgriz, N., Tran, Honghi., An Atomization Model for Splash Plate Models, *Fluid Mechanics and Transport Phenomena*, Vol. 56, No. 4, pp. 849-857.

[9] Ashgriz, N., "Handbook of Atomization and Sprays," Springer New York, 2011.